PHOTONICS Research

$SrAl_2O_4$ crystallite embedded inorganic medium with super-long persistent luminescence, thermoluminescence, and photostimulable luminescence for smart optical information storage

PANPAN LI, YOUJIE HUA, RENGUANG YE, MUZHI CAI, SHIQING XU, AND JUNJIE ZHANG*

Key Laboratory of Rare Earth Optoelectronic Materials and Devices of Zhejiang Province, Institute of Optoelectronic Materials and Devices, China Jiliang University, Hangzhou 310018, China
**Corresponding author: jjzhang@cjlu.edu.cn*

Received 23 September 2021; revised 10 November 2021; accepted 7 December 2021; posted 7 December 2021 (Doc. ID 444145); published 14 January 2022

As a leader of long persistent luminescence (LPL) materials, the optical properties of aluminate phosphor have remained unsurpassed for many years. As a powder material, its practical application will always be limited to the field of security signs. In this paper, the $SrAl_2O_4:Eu^{2+}$, Dy^{3+} inorganic solid material with comparable LPL properties to powder materials was obtained. The crystallization mechanism and crystallite micro-morphology of inorganic glass materials have been studied, and a new opinion is put forward that the large-size $SrAl_2O_4$ crystallites in the glass matrix are stacked by rod-shaped crystals arranged in a regular direction. In addition, the $SrAl_2O_4:Eu^{2+}$, Dy^{3+} glass obtained cannot only collect high-energy photons but also is sensitive to low-energy sunlight. The results show that the material exhibits superior performance in LPL, thermoluminescence, and photostimulable luminescence. Based on this property, a new application of this material in the field of information storage was explored. This paper has a certain reference value for the development and application of aluminate LPL materials in the field of smart optical information storage.

https://doi.org/10.1364/PRJ.444145

1. INTRODUCTION

The transformation of information storage has brought people into the rapidly growing "era of digital information explosion," which has stimulated updating secure storage media and various storage methods [1]. At present, optical data storage has become the new generation of information storage stars because of its advantages of high efficiency, energy conservation, environmental protection, privacy, repeatable writing, and reading [2–6].

Recently, a long persistent luminescence (LPL) medium with excellent performance has emerged and shines brightly in the field of optical data storage. Zhuang reported, for example, that spherical $NaYF_4:Ln^{3+}$ LPL nanoparticles uniformly dispersed in solvent were used to display a new 3D (2D in plane space and 1D in wavelength) optical information storage application by inkjet printing polychromatic nanoparticles [7]. In addition, Zhuang's research group proposed a surface passivation strategy of a core-shell structure to prepare $NaMgF_3:Tb^{3+}@NaMgF_3:Tb^{3+}$ nanoparticles, which effectively improved the LPL performance of nanoparticles and showed excellent optical storage capacity of deep traps under X-ray irradiation. The nanoparticles' luminescent ink with good dispersion and water stability was successfully prepared and applied to the fields of inkjet printing optical information and information decryption [8]. Wang *et al.* developed a material for embedding nanocrystal ($LiGa_5O_8:Mn^{2+}$) with photostimulable luminescence (PSL) characteristics in transparent glass ceramics, which allows bit-by-bit writing and reading optical data in photon capture and DE trapping mode with high coding/decoding resolution and low bit error rate [9].

Since Matsuzawa's discovery of green $SrAl_2O_4:Eu^{2+}$, Dy^{3+} LPL phosphor in the 1990s [10], long-lasting, bright LPL performance and potential optical applications have remained unparalleled, which also opened the prelude to the research of new LPL materials. The disadvantages of aluminate LPL material such as single preparation process, insufficient color diversity, and poor chemical stability were improved by researchers over the following years [11–15], which laid a good foundation for the development of LPL glass. Glass block materials have the advantages of controllable shape and good stability compared

with powder materials [16]. In 2015, Nakanishi adopted the "frozen sorbet" technology to separate the $SrAl_2O_4:Eu^{2+}$, Dy^{3+} crystallite phase from the liquid melt by controlling the cooling temperature at 1500°C, and obtained the $SrAl_2O_4:Eu^{2+}$, Dy^{3+} transparent glass-ceramic composite [17]. In 2016, Shinozaki obtained hexagonal β-$SrAl_2O_4$ glass and supercooled ceramic beads better than α-$SrAl_2O_4$ by controlling the cooling rate and using gas phase suspension technology [18]. In the same year, Yamashita used a two-step method to obtain LPL glass-ceramic composites by sintering $SrAl_2O_4:Eu^{2+}$, Dy^{3+} LPL phosphors in borate glass powder [19]. However, it is difficult for LPL material to realize nanosizes, which reduces micrometer resolution and limits the capacity of storage space in the process of light–matter interaction. Thus, for a $SrAl_2O_4:Eu^{2+}$, Dy^{3+} glass system with excellent LPL performance, the application scope is mainly limited in the field of safety signs but rarely in the field of big data storage. In addition, the LPL phenomenon is obtained in most research work based on the irradiation of high-energy photons such as ultraviolet (UV) light; in addition, there are few studies on the sunlight irradiation LPL, PSL phenomenon and the arrangement mode of the crystallite in glass matrix [13,20–23]. Therefore, we hope to supplement deficiencies in other research and hope to develop new applications of $SrAl_2O_4$ LPL glass.

Herein, we develop a glass ceramic via *in situ* precipitation of LPL $SrAl_2O_4:Eu^{2+}$, Dy^{3+} crystallite from a glass matrix. With the increase of B_2O_3 content, the controlled thermal driving temperature leads to the highly ordered arrangement of crystallites along the rod direction in the glass network. The continuous distribution of shallow trap levels makes the glass sensitive to photons, so the LPL phenomenon can occur even under the irradiation of low-energy light (such as sunlight and white light), and the addition of Dy^{3+} facilitates the increase of deep trap density for $SrAl_2O_4$ glass; thus, the continuous energy storage of deep trapped electrons gains the thermoluminescence (TRL) and PSL phenomena under heat stimulation and 980 nm light, respectably. Finally, the feasibility of $SrAl_2O_4:Eu^{2+}$, Dy^{3+} glass deep trap optical storage is explored by using a photomask, which demonstrates that glass obtained has the functions of writing, reading, and erasing. This work highlights broad prospects in the field of optical data information storage for $SrAl_2O_4:Eu^{2+}$, Dy^{3+} glass.

2. EXPERIMENTAL SECTION

$SrAl_2O_4$ glass samples were prepared by a melting-quenching route. The inorganic medium was elaborately designed with molar compositions of $35Sr_2CO_3$-XB_2O_3-YAl_2O_3 ($X + Y = 65$), and small amounts of rare-earth components ($0.01Eu_2O_3$–$0.005Dy_2O_3$) were added. The grounding weighed stoichiometric compounds were put into an alumina dry pot and melted at 1500°C for 1 h in an activated carbon reducing atmosphere. After that, the homogenized melt was poured onto a preheating plate at 500°C and quickly transferred to an annealing furnace at 600°C for holding 3 h to eliminate the thermal stress. The glass samples formed after reducing the annealing furnace to room temperature were named B25, B30, B35, and B40. The glass samples were finally polished to a thickness of 0.5 cm for further characterization.

An STA 449F30020 synchronous thermal analyzer was used to obtain the differential scanning curve (DSC). The crystallite phase of glass samples was identified via X-ray diffraction (XRD) measurement (D2 ADVANCE/Germany Bruker phaser diffractometer) with Cu-Kα radiation ($\lambda = 0.1541$ nm) in the 2θ range from 10° to 70° at 30 kV. The particle micromorphology and size were detected using transmission electron microscope (TEM) and high-resolution TEM (HRTEM) of FEI Tecnai F20 at 300 kV. The structure of the glass surface was observed by a scanning electron microscope (SEM) of SU 8010 SEM. Fourier transform infrared absorption (FTIA) and transmission (FTIT) spectra in the range of 400–2000 cm^{-1} were recorded by a Fourier infrared spectrometer of Nicolet iS50. The photoluminescence excitation (PLE), photoluminescence (PL), PSL, and LPL spectra were obtained via a France FL3-211 fluorescence spectrophotometer. The absorption (Abs) and transmittance (Tra) spectra in the range of 350–750 nm were measured by a UV3600 spectrophotometer. The sample was first irradiated for 5 min under UV; then, the TRL glow curve was obtained by a TOSL-3DS TRL meter with a heating rate of 5°C/s.

3. RESULTS AND DISCUSSION

DSC test was carried out on B25–B40 samples. The T_{c2} of B25 and B30 is about 1300°C (the large $SrAl_2O_4$ crystals can be obtained in the matrix by secondary heat treatment at 1300°C), which is close to its melting temperature of 1500°C [Fig. 1(a)]. According to previous reports [24], $SrAl_2O_4$ crystals can be precipitated directly from the glass matrix by *in situ* crystallization during pouring glass melt. However, T_{c2} decreases to 1000°C with the increase of B_2O_3, which is much lower than the glass melting temperature [Fig. 1(b)]; thus, $SrAl_2O_4$ crystals cannot be precipitated directly from the glass matrix during pouring glass melt. In this case, when the B35 and B40 were heat-treated at T_{c1} and T_{c2} for 2 h, respectively, the crystal phase of SrO was generated in glass matrix. It can be observed from Fig. 1(c) that the B35 and B40 samples without the $SrAl_2O_4$ crystallite display high transparency of visible light. Nevertheless, the B25 and B30 samples reveal that $SrAl_2O_4$ crystallite precipitates from the large hump of glass matrix (without secondary heat treatment), which is accurately matched with PDF card (34-0379). The Tra of the glasses was tested [Fig. 1(d)], and the results show that the transparency of the glass is gradually reduced due to the scattering of light by microcrystals. The FTIT and FTIA spectra of glass matrix were tested in Figs. 1(e) and 1(f) to further study the mechanism of *in situ* self-crystallization of a glass matrix, respectively, which complement each other and can be combined to analyze the changes of a glass internal network structure. In addition, the binding bonds represented by each vibration peak were given in the following Table 1: $[BO_4]$ is easy to change to $[BO_3]$ at high temperature. Compared with B35 and B40 glasses, the melting temperature of B25 and B30 samples increased with the decrease of B_2O_3 content. However, the actual melting temperature of all samples is kept at 1500°C, which does not lead to the complete transformation of $[BO_4]$ to

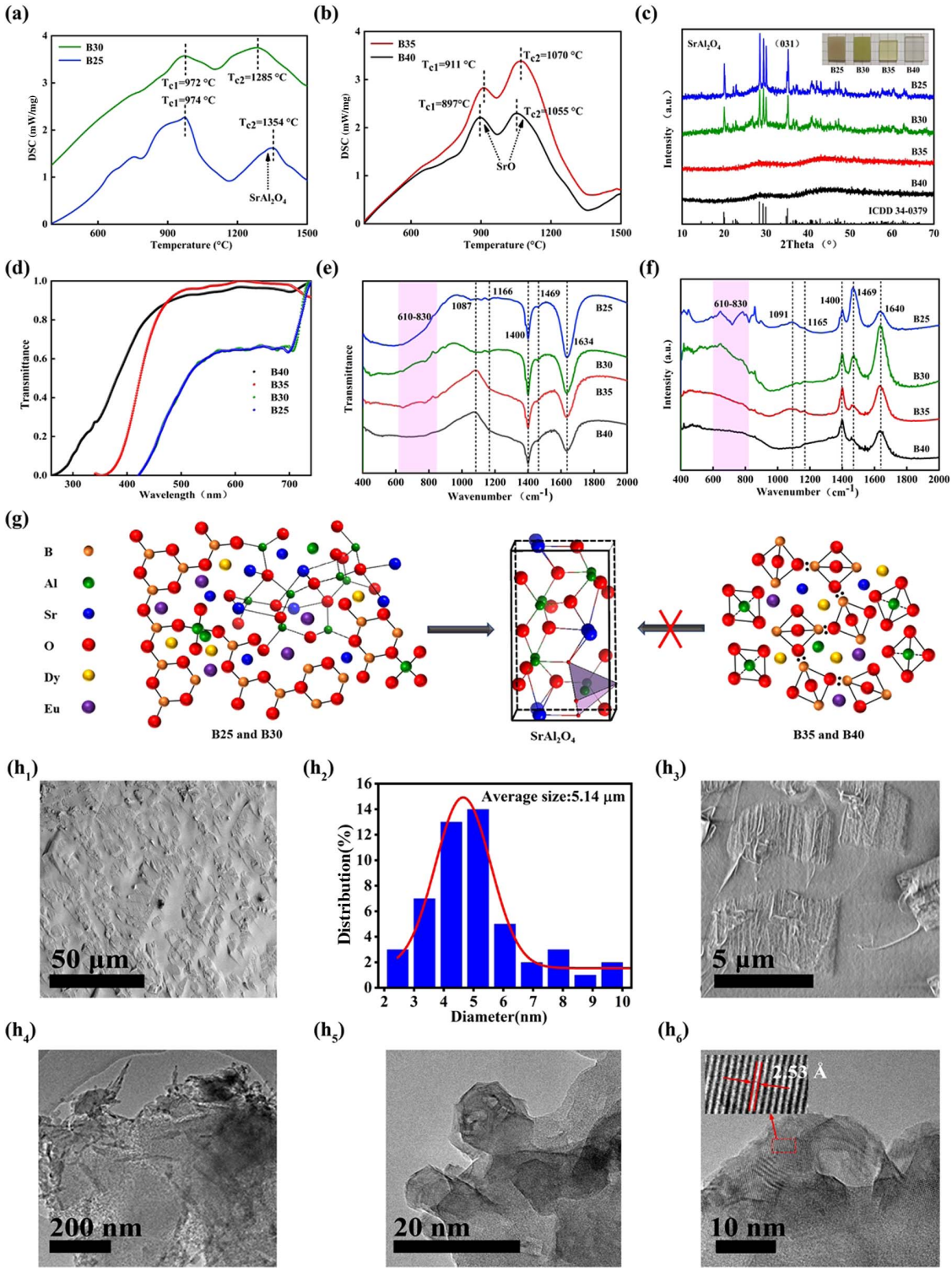

Fig. 1. Crystallization of glass samples for *in situ* precipitation of $SrAl_2O_4$ crystallites. (a) and (b) DSCs of B25–B40 samples (T_{c1} and T_{c2} represent two crystallization peaks of glass, respectively). (c) XRD patterns of different B_2O_3 doping; inset presents glass sample picture. (d) Tra spectrum of B25–B40 glass samples. (e) and (f) FTIT and FTIA spectra of glass samples, respectively. (g) Structure schematic representation of the samples. (h_1)–(h_6) The microcrystals patterns of $SrAl_2O_4$ crystallites of B30 sample, in which (h_1) and (h_3) are SEM patterns of glass surface; (h_2) shows the size distribution of the crystallite's particles; (h_4) is TEM observation; (h_5) and (h_6) are HRTEM observations.

$[BO_3]$; further, it is natural that $[BO_3]$ structural units and $[BO_4]$ structural units coexist in B25 and B30 samples, while there are only $[BO_3]$ structural units in B35 and B40 samples. Here, it is worth considering why it is difficult to produce self-crystallization in a looser network environment of B35 and B40 samples. It can be seen from Fig. 1(f) that the

Table 1. Assignment of FTIT and FTIA Spectra of Samples

Peak Position FTIT/cm^{-1}	Peak Position FTIA/cm^{-1}	Bond Type	Assignment	References
610–830	610–830	[BO_3]	Bending vibration of O-B-O	[25]
1087	1091	[BO_4]	Antisymmetric stretching vibration of O-B-O bond	[26]
1166	1165	[BO_3]	Symmetric stretching vibration of B-O bond	[27]
1400	1400	[BO_3]	Antisymmetric stretching vibration of O-B-O bond	[28]
1469	1469	Sr-O-Al	Asymmetric stretching vibration of Sr-O-Al	[29]
1634	1640	H-O	Bending vibration of OH	[26]

Sr-O-Al bond strength located at 1469 cm^{-1} decreases with the decrease of Al_2O_3, which indicates that the binding ability of Sr-O-Al is weakened, and the corresponding $SrAl_2O_4$ crystallite cannot be obtained in the looser network environment. Figure 1(g) shows a schematic diagram of the glass network structure: Al^{3+} ions are easy to combine with Sr^{2+} ions and O^{2-} ions to form $SrAl_2O_4$ crystallite *in situ* owing to the decrease of melting temperature in the glass matrix with low B_2O_3 content [17]; in the glass matrix with high B_2O_3 content, it is opposite.

Besides, Figs. 1(h_1)–1(h_6) observe the morphology of $SrAl_2O_3$ microcrystals in a glass matrix from macro to micro perspectives. First, through an SEM test of the B30 glass sample surface, it can be clearly observed that the smooth glass surface regularly grows rod-stacked crystals with a size of about 5 μm along the same direction. The larger size rod-stacked crystals are easily damaged when the sample for TEM is prepared. Therefore, rod-shaped crystals can be seen in the TEM instead of rod-stacked crystals [Fig. 1(h_4)]. Under the HRTEM [Fig. 1(h_6)], obvious lattice stripes with a lattice spacing of 2.53 Å corresponding to the (031) crystal plane can be seen.

The B25 and B30 samples growing $SrAl_2O_4$ crystallites show typical broadband PL characteristics owing to the highest fluorescence intensity at 519 nm under the excitation of 425 nm [Fig. 2(a)]. The B35 and B40 samples without $SrAl_2O_4$ crystallites show multimodal emission under the excitation of 348 nm [Fig. 2(b)]: the peak at 485 nm belongs to $4f^65d^1 - 4f^7$ transition of Eu^{2+} [24]; the peak at 575 nm belongs to the f-f transition $4F_{9/2} - 6H_{13/2}$ of Dy^{3+} [30]; the peak position at 610 nm belongs to the f-f transition $5D^0 - 7F^2$ of Eu^{3+}. This result shows that the change of glass matrix network structure has a significant effect on the local environment and luminescence properties of rare-earth ions. Furthermore, the Abs spectra were characterized in the visible range (350–750 nm), and the result shows that the absorption wavelength extends from the ultraviolet band to the infrared band, which attributes to improving the LPL performance of the glass as well as making it more sensitive to light stimulation. Notably, unabated bright green LPL in B25 and B30 samples is observed with naked eyes for 10 min after the ultraviolet light irradiation for 5 min, while the green LPL in B25 and B30 samples is weak after 3 s of observation [Fig. 2(d)].

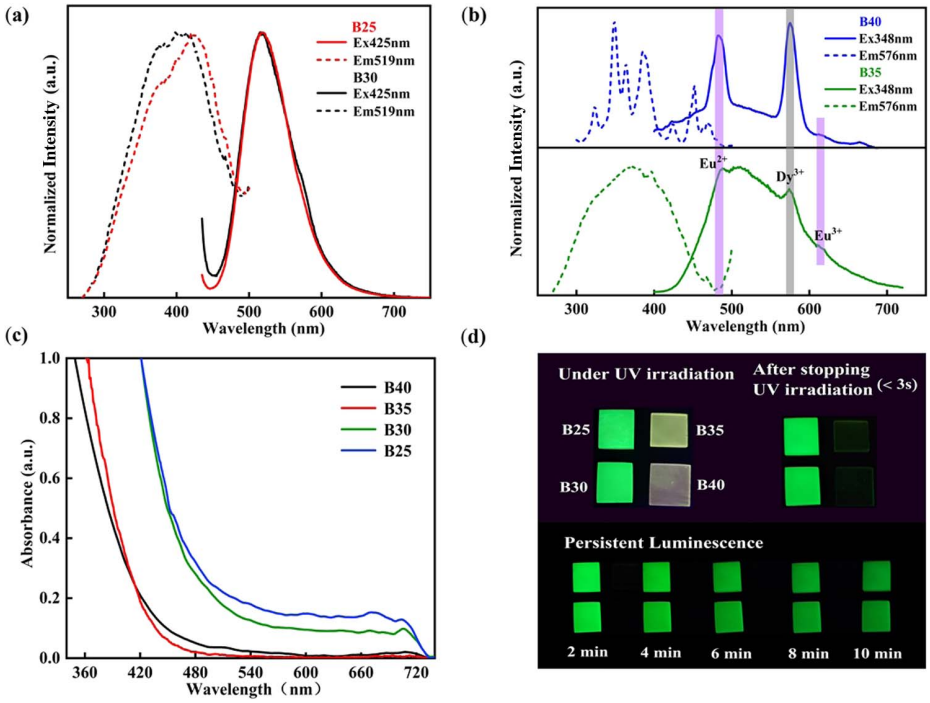

Fig. 2. PL properties of $SrAl_2O_4$ glass at room temperature. (a) PLE and PL spectra of B25 and B30 glass samples. (b) PLE and PL spectra of B35 and B40 glass samples. (c) Abs spectra of B25–B40 glass samples. (d) Photographs of B25–B40 glass samples under UV excitation and after 5 min UV light irradiation.

Through trapping of the TRL curve in Fig. 3(a), analysis reveals the LPL mechanism in the $SrAl_2O_4$ embedded B30. Four electron traps at 366 K (trap 1), 402 K (trap 2), 447 K (trap 3), and 533 K (trap 4) were fitted by Gaussian function, and trap depth E can be calculated by the following formula [31]:

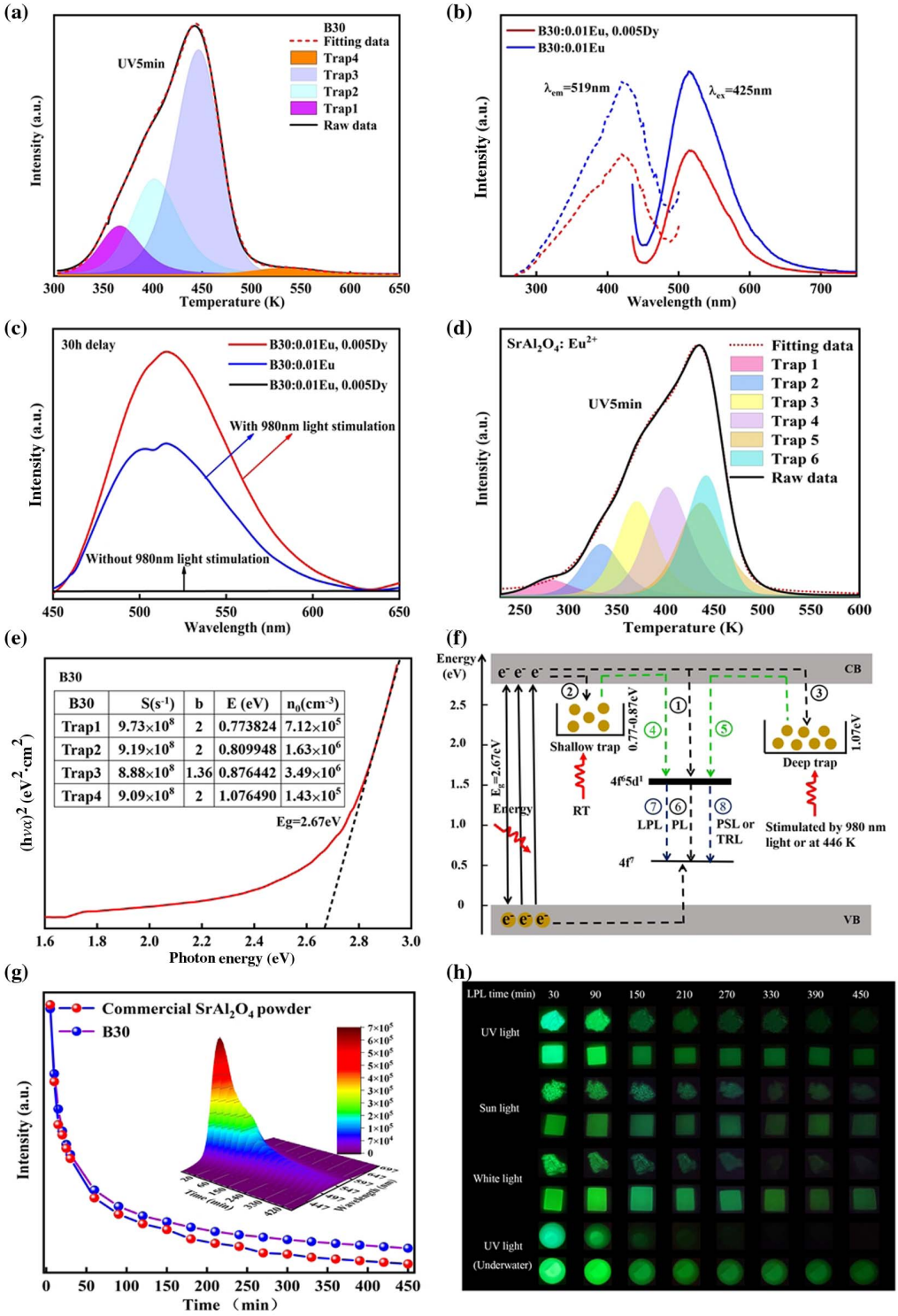

Fig. 3. LPL property and mechanism in the $SrAl_2O_4$ embedded B30. (a) TRL curve of $SrAl_2O_4$ glass after irradiation of UV light for 5 min. (b) PLE and PL spectra of B30:0.01Eu, 0.005Dy, and B30:0.01Eu samples. (c) Emission spectra of B30:0.01Eu, 0.005Dy, and B30:0.01Eu samples were first irradiated under ultraviolet light for 5 min and then excited with 980 nm light after decay time $t = 30$ h. (d) TRL curve of $B30:0.01Eu^{2+}$. (e) Diffuse reflection spectrum of the B30; inset lists the parameters about the TRL trap in (a). (f) PSL, TRL, and LPL mechanisms of the $SrAl_2O_4$ glass. (g) LPL decay curves of B30 and commercial $SrAl_2O_4$ powder; inset is LPL decay spectrum of B30 at room temperature. (h) LPL pictures of B30 and commercial $SrAl_2O_4$ powder after stopping UV irradiation.

$$E = T_m/500, \quad (1)$$

where T_m (K) is the temperature of the TRL emission peak. In addition, the frequency factor s, trap density n_0, and fitting kinetic series B were fitted via the first-order kinetic formula, as follows [32,33]:

$$I(t) = n_0 s \exp\left(-\frac{E}{kT}\right) \times \left[(b-1)(s/\beta)\int_{T_0}^{T} \exp\left(-\frac{E}{kT'}\right)dT' + 1\right]^{-\frac{b}{b+1}}, \quad (2)$$

where k (eV/J) is the Boltzmann constant, and β (K/s) is heating rate; further, the curve of $(h\nu\alpha)^2$ versus photon energy for B30 is plotted as shown in Fig. 3(e). The bandgap E_g of the glass matrix is 2.67 eV; the other relevant parameters mentioned above are also listed in the inset of Fig. 3(e). Obviously, there are shallow traps (0.77–0.87 eV) and deep traps (>1 eV) in B30 samples. Generally, the trap depth of 0.5–0.8 eV is considered as an ideal LPL material, while it should exceed 1.2 eV for PSL [34]. It can be inferred from the distribution of trap density n_0 that most electrons are captured by shallow traps, and a few electrons are captured by the deep trap in the $SrAl_2O_3$ glass, as discussed in this paper. As a result, the bright LPL characteristics at the shallow trap in the material can be observed at room temperature. After the LPL decays to invisible to the naked eye, the weak TRL and PSL characteristics coming from electrons at the deep trap can be observed under the stimulation of thermal and 980 nm light. As we all know, LPL can also be obtained by adding Eu^{2+} to $SrAl_2O_4$ crystallite. The spectra when Dy^{3+} ions are added were detected to explain the effect of co-doped rare-earth on LPL. As shown in Figs. 3(b) and 3(c), similar PL characteristics are shown in B30:0.01Eu, 0.005Dy, and B30:0.01Eu under 425 excitation. However, the PL intensity of B30:0.01Eu, 0.005Dy is much lower than that of B30:0.01Eu. As expected, the B30:0.01Eu, 0.005Dy, and B30:0.01Eu samples were first irradiated under UV light for 5 min and then excited with 980 nm light after placed in the dark room for 30 h. The result shows that the PL intensity of B30:0.01Eu, 0.005Dy is much higher than that of B30:0.01Eu. The TRL curve of B30:0.01Eu was further tested to support the above inference. Obviously, Fig. 3(d) shows that the trap depth (<1.0 eV) is greatly weakened when only Eu^{2+} is added to the glass. Similarly, this phenomenon indicates that the addition of Dy^{3+} ions increases the density of the deep trap, and more electrons can be captured by the deep trap, thus reducing the PL intensity under the excitation of 425 nm, while the electrons at the deep trap can be released under secondary excitation (980 nm), resulting in the increase of PSL intensity.

The proposed energy-level diagram for explaining the charge carrier transition process in $SrAl_2O_4$ glass during and after UV irradiation is shown in Fig. 3(f). $SrAl_2O_4$ crystallites are uniformly distributed in the glass matrix with an energy bandgap of 2.67 eV; further, there are two trap levels between the conduction and valence bands of the sample co-doped with Eu^{2+} and Dy^{3+}. Electrons located in the valence band of the glass matrix will be excited to the conduction band under the action of light, and these electrons will be captured through three paths. The electrons captured by Process (1) are located at the 5d level of Eu^{2+}, which can directly transition to the 4f level and emit the characteristic yellow-green PL of Eu^{2+} ions [Process (6)]. After cutting off the light source, a large number of electrons can be captured to the shallow trap level by Process (2). These electrons can escape to the 5d level of Eu^{2+} at room temperature through Process (4), producing bright and lasting green LPL after transitioning to the 4f level [Process (7)].

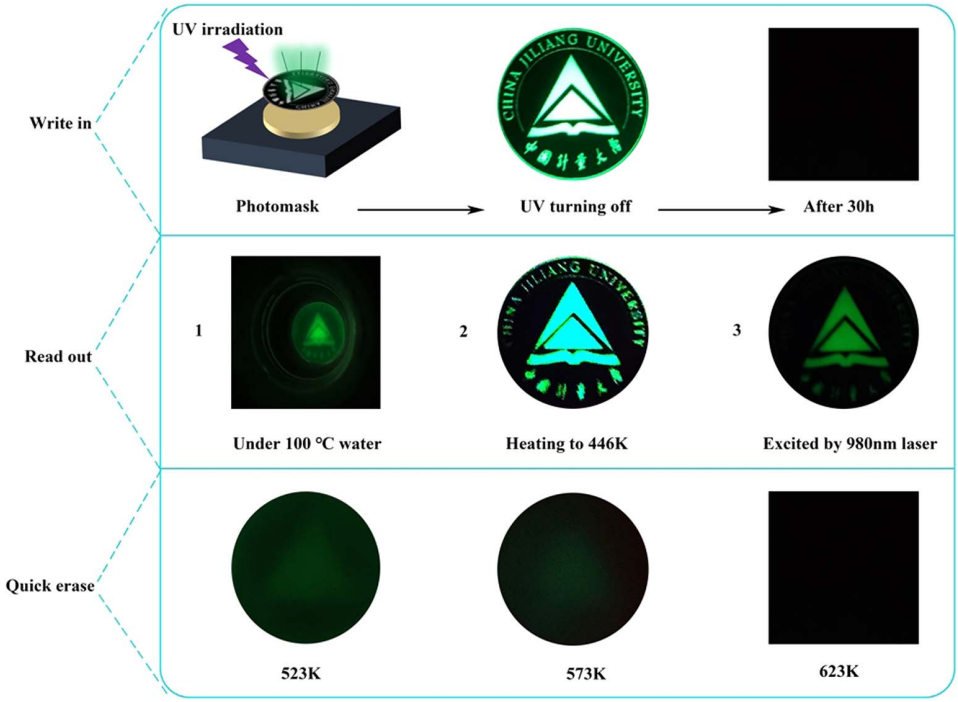

Fig. 4. Glass pictures of writing, reading, and erasing processes of optical information.

A small number of electrons can be captured to the deep trap by Process (3). However, external high-temperature thermal stimulation or 980 nm light stimulation, results in weak green TRL or PSL [Process (8)] and displays the stored information in the form of photon emissions. (It should be noted that the intensity of LPL, TRL, and PSL is determined by the trap density n_0.) Aiming to evaluate the application potential of $SrAl_2O_4$ glass prepared in this work, green $SrAl_2O_4$ commercial LPL phosphor was purchased for performance comparison. After 30 min of excitation under UV light, the LPL curve in Fig. 3(g) exhibits identical change tendency with that of LPL picture [Fig. 3(h)], where the B30 sample shows the intense LPL output, lasting more than 450 min. Actually, the LPL time of B30 can be observed by the naked eye for up to 28 h. However, the fluorescence intensity of commercial phosphors is much lower than that of our material after 150 min. In addition, in Fig. 3(h), after the glass and commercial phosphor were irradiated either under UV light, sun light, or white light for 30 min, one can see that the LPL intensity of the glass sample is still higher than that of commercial phosphor after attenuation of 450 min. In addition, the water stability between glass and commercial phosphors was also compared. After they were placed in water and irradiated under the UV light for 30 min, the commercial LPL phosphor cannot yield the LPL after 270 min in a dark room. The above experimental results show that the $SrAl_2O_4$ glass prepared in this work has superior LPL properties and water stability, indicating that the $SrAl_2O_4$ glass can be applied in the fields of indication and information storage.

Figure 4 explores the potential application of glass in the field of information storage. A special photomask is irradiated by UV light, and the information of the photomask is stored in the glass in the form of photons. The optical information was engraved into the glass after turning off the UV light source, which is unrecognizable after being placed in a dark room for 30 h. The information can be read out again in the following three methods. (i) Place the glass in 100°C water or (ii) place the glass in a furnace at about 440 K. Both methods are to release the electrons of the deep trap through thermal stimulation. (iii) Release the electrons of the deep trap through optical stimulation under 980 nm light irradiation (surface scanning irradiation). Finally, this optical information can be quickly eliminated without a long wait, i.e., placing the glass in a furnace higher than 663 K, which will completely release the electrons in the deep trap and return the sample to its original state.

4. CONCLUSION

In summary, $SrAl_2O_4:Eu^{2+}$, Dy^{3+} embedded in inorganic medium was successfully developed as stable LPL, TRL, and PSL materials by *in situ* crystallization method. The network structure of glass and the arrangement mode of $SrAl_2O_4$ crystallite were studied. It is considered that the $SrAl_2O_4$ crystallite is regularly arranged and stacked along the rod direction in the glass matrix and finally exists in the glass in the form of crystallite with a size of 5 μm. In addition, the mechanism of LPL, TRL, and PSL was studied. The results show that doping Dy^{3+} in the glass matrix strengthens the trap density, prolonging the LPL time and providing more electrons in deep trap for TRL and PSL. Compared with commercial $SrAl_2O_4$ LPL phosphors, the LPL attenuation time of glass is longer than 25 h with excellent water-resistance stability. Finally, the prepared $SrAl_2O_4$ glass with write-in, read-out, and erase functions offers bright prospects in the application field of optical information storage.

Funding. Key Laboratory of Rare Earth Optoelectronic Materials and Devices of Zhejiang Province of China; National Natural Science Foundation of China (62075204, U1909211).

Acknowledgment. We thank Yongmin Duan and Yang Lu for providing constructive criticism for this paper.

Disclosures. The authors declare no conflicts of interest.

Data Availability. Data underlying the results presented in this paper are not publicly available at this time but may be obtained from the authors upon reasonable request.

REFERENCES

1. M. Gu, X. Li, and Y. Cao, "Optical storage arrays: a perspective for future big data storage," Light Sci. Appl. **3**, e177 (2014).
2. W. Zhang, X. Liu, Q. Li, H. Tang, J. Xie, Z. Wang, C. Wang, L. Jiang, and X. Zhang, "Excellent thermal stability of $Y_{2.94}Al_{4-x}Si_xGaO_{12}$:0.06$Ce^{3+}$ phosphor for optical storage," J. Alloys Compd. **880**, 160220 (2021).
3. X. Lin, K. Deng, H. Wu, B. Du, B. Viana, Y. Li, and Y. Hu, "Photon energy conversion and management in $SrAl_{12}O_{19}$: Mn^{2+}, Gd^{3+} for rewritable optical information storage," Chem. Eng. J. **420**, 129844 (2021).
4. Z. Long, J. Zhou, J. Qiu, Q. Wang, Y. Li, J. Wang, D. Zhou, Y. Yang, H. Wu, and Y. Wen, "Thermal engineering of electron-trapping materials for "Smart-Write-In" optical data storage," Chem. Eng. J. **420**, 129788 (2021).
5. P. Wen, Y. Xu, S. Li, Z. Sun, M. Panmai, J. Xiang, S. Tie, and S. Lan, "Two-dimensional closely-packed gold nanoislands: a platform for optical data storage and carbon dot generation," Appl. Surf. Sci. **555**, 149586 (2021).
6. Z. Hu, X. Huang, Z. Yang, J. Qiu, Z. Song, J. Zhang, and G. Dong, "Reversible 3D optical data storage and information encryption in photo-modulated transparent glass medium," Light Sci. Appl. **10**, 140 (2021).
7. Y. Zhuang, D. Chen, W. Chen, W. Zhang, X. Su, R. Deng, Z. An, H. Chen, and R. J. Xie, "X-ray-charged bright persistent luminescence in $NaYF_4$:Ln^{3+}@$NaYF_4$ nanoparticles for multidimensional optical information storage," Light Sci. Appl. **10**, 132 (2021).
8. Y. Wang, D. Chen, Y. Zhuang, W. Chen, H. Long, H. Chen, and R. J. Xie, "$NaMgF_3$:Tb^{3+}@$NaMgF_3$ nanoparticles containing deep traps for optical information storage," Adv. Opt. Mater. **9**, 2100624 (2021).
9. S. Lin, H. Lin, C. Ma, Y. Cheng, S. Ye, F. Lin, R. Li, J. Xu, and Y. Wang, "High-security-level multi-dimensional optical storage medium: nanostructured glass embedded with $LiGa_5O_8$:Mn^{2+} with photostimulated luminescence," Light Sci. Appl. **9**, 22 (2020).
10. T. Matsuzawa, Y. Aoki, N. Takeuchi, and Y. Murayama, "A new long phosphorescent phosphor with high brightness, $SrAl_2O_4$:Eu^{2+}, Dy^{3+}," J. Electrochem. Soc. **143**, 2670–2673 (2019).
11. Z. Xue, S. Deng, and Y. Liu, "Synthesis and luminescence properties of $SrAl_2O_4$:Eu^{2+}, Dy^{3+} nanosheets," Physica B **407**, 3808–3812 (2012).
12. Y. F. Xu, D. K. Ma, M. L. Guan, X. A. Chen, Q. Q. Pan, and S. M. Huang, "Controlled synthesis of single-crystal $SrAl_2O_4$:Eu^{2+}, Dy^{3+} nanosheets with long-lasting phosphorescence," J. Alloys Compd. **502**, 38–42 (2010).

13. H. Song and D. Chen, "Combustion synthesis and luminescence properties of $SrAl_2O_4$:Eu^{2+}, Dy^{3+}, Tb^{3+} phosphor," Luminescence **22**, 554–558 (2007).
14. S. Yu, P. Pi, X. Wen, J. Cheng, and Z. Yang, "Preparation and luminescence of $SrAl_2O_4$:Eu^{2+}, Dy^{3+} phosphors coated with maleic anhydride," Can. J. Chem. Eng. **86**, 30–34 (2008).
15. J. M. Ngaruiya, S. Nieuwoudt, O. M. Ntwaeaborwa, J. J. Terblans, and H. C. Swart, "Resolution of Eu^{2+} asymmetrical emission peak of $SrAl_2O_4$:Eu^{2+}, Dy^{3+} phosphor by cathodoluminescence measurements," Mater. Lett. **62**, 3192–3194 (2008).
16. P. Roldán Del Cerro, T. Salminen, M. Lastusaari, and L. Petit, "Persistent luminescent borosilicate glasses using direct particles doping method," Scr. Mater. **151**, 38–41 (2018).
17. T. Nakanishi, "Preparation of europium-activated $SrAl_2O_4$ glass composites using the frozen sorbet technique," J. Ceram. Soc. Jpn. **123**, 862–867 (2015).
18. K. Shinozaki, T. Honma, M. Affatigato, and T. Komatsu, "Long afterglow in hexagonal $SrAl_2O_4$:Eu^{2+}, Dy^{3+} synthesized by crystallization of glass and solidification of supercooled melts," J. Lumin. **177**, 286–289 (2016).
19. M. Yamashita, T. Imamura, S. Matsumoto, M. Murakami, T. Hongo, T. Akai, and Y. Iwamoto, "Enhancement of afterglow luminescence of long-lasting phosphor-glass composite by using refractive index matched glass," Key Eng. Mater. **702**, 113–117 (2016).
20. H. Yoshida, S. Fujino, and T. Kajiwara, "Afterglow luminance property of phosphorescent phosphor $SrAl_2O_4$:Eu^{2+}, Dy^{3+}-glass composites," J. Ceram. Soc. Jpn. **118**, 784–787 (2010).
21. B. Cheng, Z. Zhang, Z. Han, Y. Xiao, and S. Lei, "$SrAl_2O_4$:Eu^{2+}, Dy^{3+} nanobelts: synthesis by combustion and properties of long-persistent phosphorescence," J. Mater. Res. Technol. **26**, 2311–2315 (2011).
22. Y. Wu, J. Gan, and X. Wu, "Study on the silica-polymer hybrid coated $SrAl_2O_4$:Eu^{2+}, Dy^{3+} phosphor as a photoluminescence pigment in a waterborne UV acrylic coating," J. Mater. Res. Technol. **13**, 1230–1242 (2021).
23. T. Cai, S. Guo, Y. Li, D. Peng, X. Zhao, W. Wang, and Y. Liu, "Ultrasensitive mechanoluminescent ceramic sensor based on air-plasma-sprayed $SrAl_2O_4$:Eu^{2+}, Dy^{3+} coating," Sens. Actuators A **315**, 112246 (2020).
24. T. Nakanishi, Y. Katayama, J. Ueda, T. Honma, S. Tanabe, and T. Komatsu, "Fabrication of Eu:$SrAl_2O_4$-based glass ceramics using frozen sorbet method," J. Ceram. Soc. Jpn. **119**, 609–615 (2011).
25. X. Xu, Y. Wang, C. Zu, and P. Zhou, "Effect of 3B group in rings on special dispersion of B_2O_3-SiO_2-ZrO_2-Ta_2O_5-Na_2O system glass," J. Wuhan Univ. Technol. **33**, 1032–1038 (2018).
26. K. Ding, N. Chen, G. Du, and A. Zhang, "Preparation, structures, thermal properties and sintering behaviors of B_2O_3-SiO_2-ZnO-BaO-Al_2O_3 glass," J. Wuhan Univ. Technol. **31**, 1323–1328 (2016).
27. Y. Duan, P. Li, Y. Lu, S. Xu, and J. Zhang, "Enhanced luminescence of self-crystallized Cs_4PbBr_6 quantum dots via regulating glass ceramic network structure," Ceram. Int. **47**, 24198–24206 (2021).
28. J. Cui, X. Cao, L. Shi, Z. Zhong, P. Wang, and L. Ma, "The effect of substitution of Al_2O_3 and B_2O_3 for SiO_2 on the properties of cover glass for liquid crystal display: structure, thermal, visco-elastic, and physical properties," Int. J. Appl. Glass Sci. **12**, 443–456 (2021).
29. O. Sherstyuk, A. Ivanova, M. Lebedev, M. Bukhtiyarova, L. Matvienko, A. Budneva, A. Simonov, and V. Yakovlev, "Transesterification of rapeseed oil under flow conditions catalyzed by basic solids: M-Al(La)-O (M = Sr, Ba), M-Mg-O (M = Y, La)," Appl. Catal. A **419-420**, 73–83 (2012).
30. J. Xu, Z. Chen, M. Gai, Y. Fan, and C. He, "Optically stimulated luminescence of Dy^{3+}-doped $NaCaPO_4$ glass-ceramics," J. Rare Earths **38**, 927–932 (2020).
31. C. Wang, Y. Jin, Y. Lv, G. Ju, D. Liu, L. Chen, Z. Li, and Y. Hu, "Trap distribution tailoring guided design of super-long-persistent phosphor Ba_2SiO_4:Eu^{2+}, Ho^{3+} and photostimulable luminescence for optical information storage," J. Mater. Chem. C **6**, 6058–6067 (2018).
32. R. Chen, "On the calculation of activation energies and frequency factors from glow curves," J. Appl. Phys. **40**, 570–585 (1969).
33. Y. Jia, W. Sun, R. Pang, T. Ma, D. Li, H. Li, S. Zhang, J. Fu, L. Jiang, and C. Li, "Sunlight activated new long persistent luminescence phosphor $BaSiO_3$:Eu^{2+}, Nd^{3+}, Tm^{3+}: optical properties and mechanism," Mater. Des. **90**, 218–224 (2016).
34. W. Wang, J. Yang, Z. Zou, J. Zhang, H. Li, and Y. Wang, "An isolated deep-trap phosphor for optical data storage," Ceram. Int. **44**, 10010–10014 (2018).